Intrinsic anisotropy-defined magnetization reversal in submicron ring magnets

S. P. Li, W. S. Lew, J. A. C. Bland, M. Natali, A. Lebib, and Y. Chen

Citation: Journal of Applied Physics **92**, 7397 (2002); doi: 10.1063/1.1518765
View online: http://dx.doi.org/10.1063/1.1518765
View Table of Contents: http://scitation.aip.org/content/aip/journal/jap/92/12?ver=pdfcov
Published by the AIP Publishing

Intrinsic anisotropy-defined magnetization reversal in submicron ring magnets

S. P. Li, W. S. Lew, and J. A. C. Bland[a)]
Cavendish Laboratory, University of Cambridge, Madingley Road, Cambridge CB3 0HE United Kingdom

M. Natali, A. Lebib, and Y. Chen
Laboratoire de Photonique et de Nanostructures, CNRS-LPN, Route de Nozay, 91460 Marcoussis, France

(Received 11 June 2002; accepted 10 September 2002)

We report a study of the effect of magnetocrystalline anisotropy in the magnetization reversal of submicron Co rings fabricated by nanoimprint lithography. For weak magnetocrystalline anisotropy, the complete reversal takes place via a transition from saturation at large negative fields, into a vortex configuration at small fields, and back to reverse saturation at large positive fields. When the anisotropy strength is increased to a critical value, the intermediate vortex configuration no longer exists in the magnetization reversal along the easy axis; instead, the reversal occurs through a rapid jump. However, when the applied field direction is far from the easy axis, the presence of the magnetocrystalline anisotropy favors local vortex nucleation, and this leads to a similar switching process as found for low anisotropy. Micromagnetic simulations indicate that the magnetization reversal process of the rings, starts from a buckling-like reverse domain nucleation, followed by local vortex formation and an avalanche process of local vortex nucleation. © *2002 American Institute of Physics.* [DOI: 10.1063/1.1518765]

I. INTRODUCTION

Nanoscale magnetism of patterned magnetic elements has provided a great deal of scientific interest leading to potential technological applications.[1] Recent lithographic technologies have rendered possible the design and control of the magnetic properties by patterning the materials on micron or nanoscales. While nanoscale patterned magnets with various geometries, such as squares,[2,3] disks,[4,5] and wires[6,7] are being studied extensively, ring-shaped magnetic elements have generated considerable interest due to their unique features.[8,9] A ring-shaped nanoscale magnet with a flux-closure/vortex magnetic configuration generates no external magnetic fringing field, in contrast to other patterned magnetic structures;[10] thus, the ring elements can be packed very closely for ultrahigh density magnetic storage and can provide a well-defined switching field. Potential applications, for instance, the vertical magnetoresistive random access memory, based on a ring-shaped magnetic multilayer stack, have been proposed.[10,11]

A simple and well-defined magnetic configuration is an important reversal property in understanding the energetic competition in a nanoscale magnetic structure. For a square nanomagnet there exist various magnetization configurations, such as the leaf state, the flower state, the buckle state, etc.[12,13] In a disk-shaped nanomagnet, the magnetic configurations, for instance, the vortex state,[14] are less varied. However, the perpendicularly magnetized core in the vortex state poses a complicated spin distribution to the disk.[4,15,16] On the other hand, the ring-shaped nanomagnet, in fact, is a disk with its core removed. Without the perpendicularly magnetized vortex core,[4,15,16] the formation mechanism for the magnetic configuration in the ring is simple and easily expressed.

Recently, two types of lithographically patterned ring magnets have been reported. One is a mesoscopic fcc Co narrow ring with a large hole, in which the magnetization can reach full circulation.[8] Energetically, the narrow ring is similar to a wire-shaped magnet with two ends connected; the head-to-head and tail-to-tail domains appear at opposite sides of the ring. Two stable states were reported in the ring, namely, the vortex state and the bi-domain state.[8] Another type is a nanoscale polycrystalline wide ring with a small hole, which can be approximated to a nanoscale disk with its core removed. Li *et al.* have given a detailed study on the size dependence of the magnetic configuration in the wide ring,[9] in which the magnetization reversal property is defined by the competition of the exchange and magnetostatic energies. In the wide ring, a stable flux-closure/vortex state and a metastable near single-domain state were found during the reversal process in an in-plane applied field. The narrow and wide rings have distinct characteristics: for instance, the wide ring undergoes a process of local vortex nucleation before evolving into the vortex state, whereas the narrow ring reaches the vortex state through a nucleation-free process.

In this article, we address the effect of the magnetocrystalline anisotropy on the magnetic configuration and reversal properties in a submicron Co wide ring. Molecular beam epitaxy was used to produce a hcp Co ring with strong magnetocrystalline anisotropy, while a sputter-deposited polycrystalline Co ring with a very weak intrinsic anisotropy was used for comparison. Magneto-optical Kerr effect (MOKE) magnetometry and magnetic force microscopy (MFM) imaging, in conjunction with numerical micromagnetic simulations, have been used to investigate the effect of the intrinsic

a)Electronic mail: jacb1@phy.cam.ac.uk

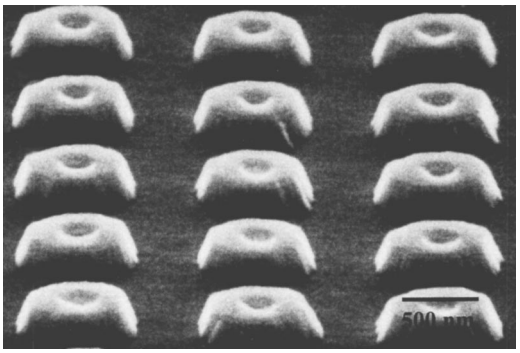

FIG. 1. SEM image of epitaxial Co rings. The GaAs substrate was deeply etched using ion milling, to ensure complete magnetic isolation between the ring nanomagnets.

anisotropy on the magnetization reversal process. Depending on the anisotropy strength and the external field direction, the magnetocrystalline anisotropy can resist or favor local vortex nucleation, leading to different reversal processes. When a field is applied near the easy axis direction, the magnetocrystalline anisotropy tends to stabilize a single-domain magnetic configuration. However, when a field is applied far from the easy axis direction, the reversal process is mediated by a vortex magnetic configuration.

II. EXPERIMENTAL PROCEDURE

A 20-nm-thick epitaxial hcp Co film, with 2-nm-thick Cu and 3-nm-thick Au protection layers, was grown on a GaAs(100) substrate, in an ultrahigh vacuum chamber (10^{-10} mbar) by electron beam evaporation. The details of the epitaxial growth and structural analyses of Co on GaAs have been reported elsewhere.[17] The mold with the ring structure used for the nanoimprint lithography was fabricated by electron beam lithography and reactive ion etching on a silicon dioxide. The sample was first coated with a 180-nm-thick hybrane polymer layer.[18] The mold and sample were then heated to 140 °C for 10 min, and then pressed against each other. After cooling down, the sample was released from the mold, and the pattern was thus replicated into the polymer, with a thickness contrast. O_2 plasma anisotropic etching was used to transfer the pattern through the entire resist thickness. The magnetic structure was defined by lift-off using 30-nm-thick Al, and pattern transfer by ion milling. The polycrystalline rings were fabricated by patterning of the resist and direct lift-off of Co. Both types of rings were arranged in an array of 160 μm$\times$160 μm size, with a separation equal to the outer diameter. Morphology observations by scanning electron microscopy (SEM) and atomic force microscopy revealed no major differences between the polycrystalline and the epitaxial ring. Also, MOKE measurements were performed on an unpatterned epitaxial hcp Co film, before and after heating at 140 °C: no significant change was found in the measured MOKE hysteresis loops.

III. RESULTS AND DISCUSSION

Figure 1 shows a SEM image of the epitaxial Co rings with outer and inner diameters of 600 nm and 200 nm, respectively. For the simplicity of the mold fabrication, and to enable the vortex magnetic configuration be visible in the scanned MFM images, all rings have an octagonal rather than a perfect circular shape. Figure 2 presents the longitudinal MOKE hysteresis loops obtained at room temperature.

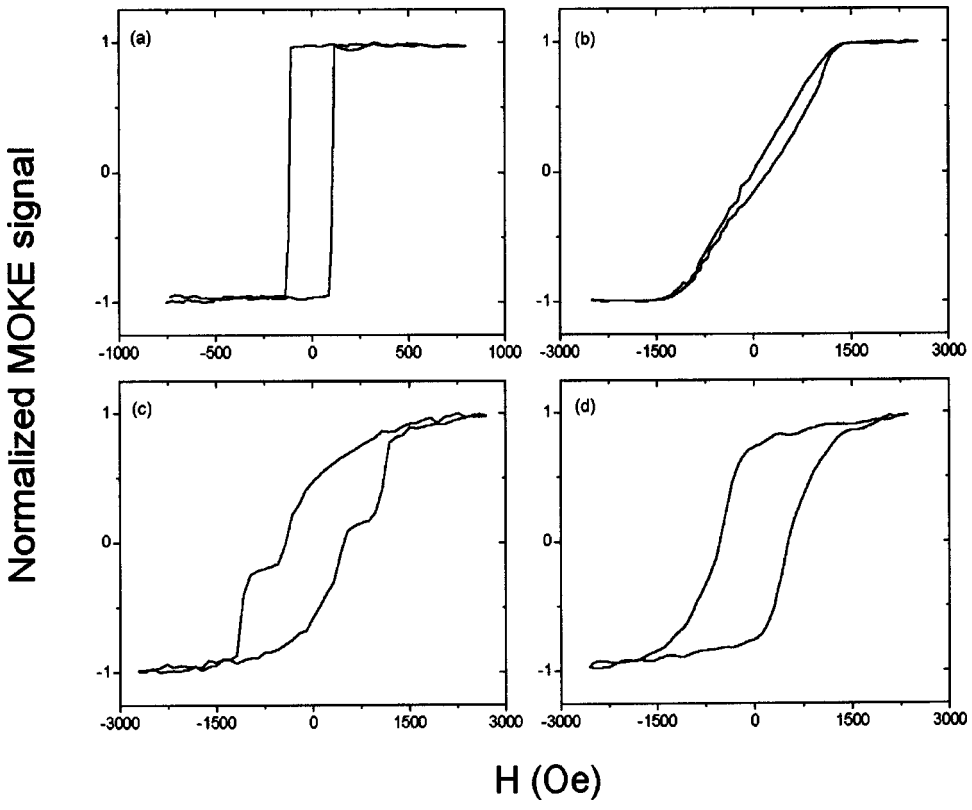

FIG. 2. Typical MOKE hysteresis loops measured at room temperature: (a) and (b) were measured along the easy and the hard axis of an unpatterned epitaxial Co film, respectively; (c) and (d) were obtained from the polycrystalline and epitaxial ring magnets, respectively.

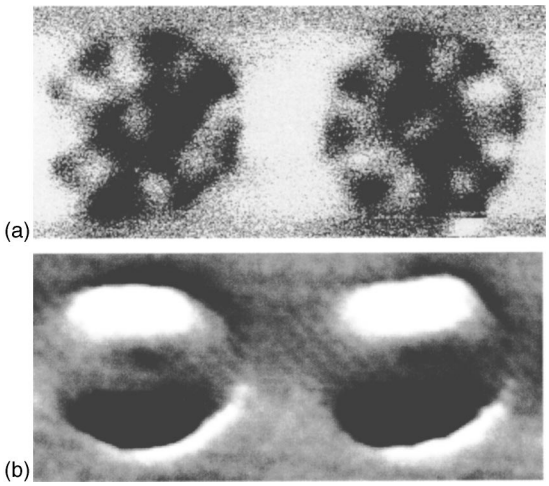

FIG. 3. MFM images of (a) polycrystalline and (b) epitaxial ring nanomagnets, obtained after applying a saturation field. For the epitaxial rings, the field was applied along the easy axis. All the images were scanned at a lift scan height of 50 nm at zero applied fields. In the polycrystalline rings, the weak contrast, with alternating bright and dark segments, indicates a vortex magnetic configuration, which is caused by the influence of the stray field of the MFM tip. The strong black and white contrast in the epitaxial rings signifies a single-domain magnetic configuration.

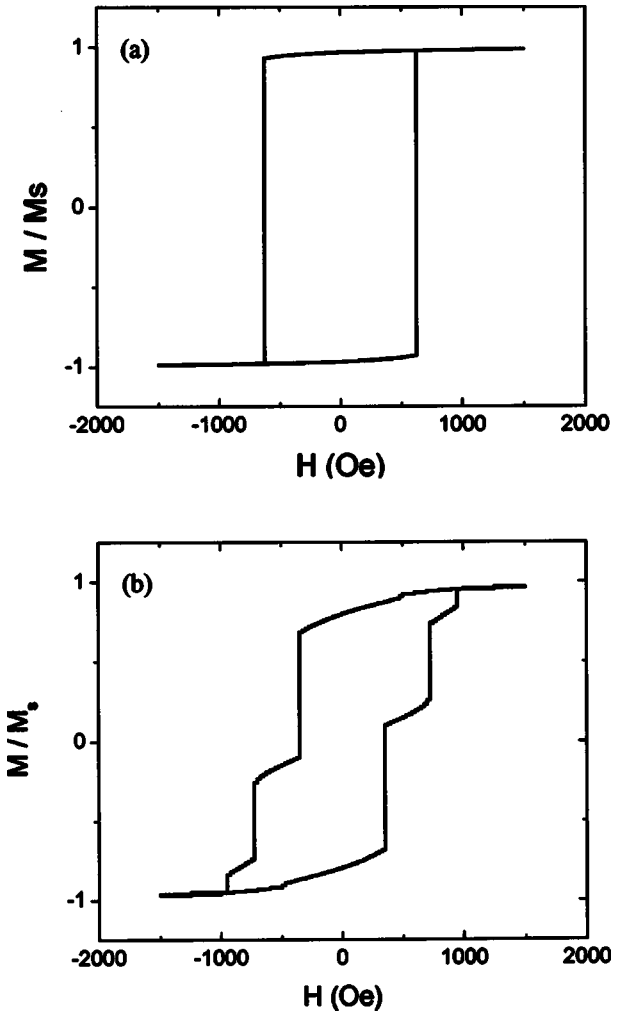

FIG. 4. Simulated hysteresis loops for (a) epitaxial and (b) polycrystalline rings, with the parameters as in our experiment.

While a perfect square hysteresis loop was obtained along the easy axis (a), a hysteresis loop with a large saturation field was observed along the hard axis, in measurements of the unpatterned film (b). This implies that a strong in-plane uniaxial magnetic anisotropy exists in the unpatterned epitaxial Co film. Loops (c) and (d) were taken from the polycrystalline and epitaxial ring samples, respectively, with a field applied along the easy axis. The most striking difference between their hysteresis behaviors is that the epitaxial rings have a nearly square loop, whereas the polycrystalline rings have a multi-jumped loop. In the polycrystalline ring loop, the first switch, at low field, is caused by the formation of a vortex magnetic configuration, in which the total energy (anisotropy, demagnetizing, and exchange) is at its minimum. The complete reversal takes place via the transformation from the single domain state, at large negative fields, into the vortex state at relatively small fields (500~1000 Oe), back into the reverse single domain state at large positive fields. In contrast, in the epitaxial ring loop, there is only a rapid switch, indicating that no vortex magnetic configuration is present in the magnetization reversal.

Figure 3 shows MFM images for the two types of rings in remanent states after being saturated with an in-plane field. The lift scan height was held at 50 nm, and with such a low scan height, the magnetic tip stray field is strong enough to switch the magnetization of the polycrystalline ring into the vortex magnetic configuration, as indicated by the weak contrast with alternating bright and dark segments in Fig. 3(a). However, the strong black and white contrast in Fig. 3(b) signifies a single-domain magnetic configuration in the epitaxial rings, which is not affected by the tip perturbation. The MFM results agree well with the MOKE measurements.

To assist our understanding of the effect of the intrinsic anisotropy in the ring magnetization, two-dimensional (2D) numerical micromagnetic simulations[9,19] have been carried out. Figure 4 shows the calculated hysteresis loops for the polycrystalline and epitaxial rings with the parameters as in the experiment. The shape of the experimental hysteresis loops [Figs. 2(c) and 2(d)] is qualitatively well reproduced by the simulations. The imperfect squareness of the experimental hysteresis loops in Fig. 2(d) is caused by defect distributions in the array of nanomagnets.[20]

To understand how the reversal mechanism is affected by the magnetocrystalline anisotropy strength, one has to first observe the reversal process in an isotropic ring in detail. Figure 5 shows the simulated magnetization vector fields in a single polycrystalline Co ring at three different stages. As the applied field strength is reduced from negative saturation, the ring nanomagnet retains a high remanence until a field near zero, where the nucleation of reverse domains starts to occur [Fig. 5(a)]. As the external field increases from zero, the nucleated reverse domain progressively evolves into a local vortex structure. The growth and displacement of the local vortex structure are accompanied by the nucleations of new local vortices, which are activated by the stray fields of the initial local vortices, in the neighboring region [Fig. 5(b)]. Such a vortex nucleation avalanche continues until the magnetization in one branch of the ring is reversed. Conse-

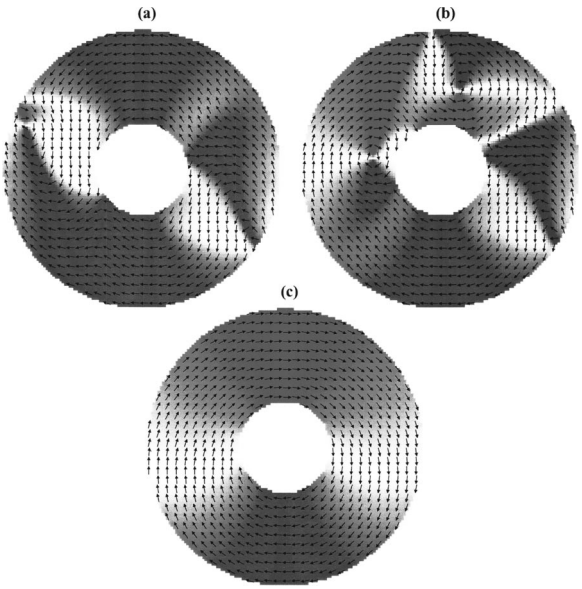

FIG. 5. Simulated magnetic configurations in the reversal process of polycrystalline Co ring. The processes are: (a) local vortex nucleation, (b) growth and displacement of local vortices, and (c) completion of vortex.

quently, the complete vortex magnetic configuration is formed in the ring nanomagnet [Fig. 5(c)]. This process corresponds to the first switch in the hysteresis loop of the polycrystalline ring.

A similar nucleation process of local vortex is experienced in the reversal of the magnetization from the vortex magnetic configuration to positive saturation, where a reverse domain is nucleated in the branch with magnetization against the external field direction. The magnetic configuration in the polycrystalline ring is defined by the competition between the demagnetizing and exchange energies. In an isotropic ring, with the scale used in the present study, the vortex magnetic configuration is energetically favorable. However, a metastable single-domain state can also be reached near zero fields, as indicated by the high remanence in the hysteresis loop [Fig. 2(c)]. Before the formation of the vortex magnetic configuration, both the exchange and demagnetizing energies of the ring progressively increase during the local vortex nucleation process (see Fig. 6). Consequently, an energy barrier is formed, and a local minimum in the total energy defines the metastable single-domain configuration. An increased external field is required to overcome this barrier in order to reach the stable vortex magnetic configuration.

While the magnetic properties of the polycrystalline rings are controlled by the shape anisotropy, the presence of the strong magnetocrystalline anisotropy, which will compete with the shape anisotropy, clearly has a significant influence on the magnetization reversal mechanism in the epitaxial rings. As mentioned earlier, the hysteresis behavior has been changed from a multi-jumped loop to a near-square loop. The question arises as to the reversal mechanism in the presence of a strong anisotropy, such as domain wall motion,[21] buckling,[22] coherent rotation,[14] etc. In order to explore the dominant mechanism, we have undertaken micromagnetic simulations of a single epitaxial ring. The simulated magnetic configurations in the reversal process of the epitaxial ring are shown in Fig. 7. A buckling-like reversal mechanism that starts at the edge of the ring has been found [Fig. 7(a)]. The process for the local vortex formation from a reverse domain, followed by nucleation avalanche of local vortices [Fig. 7(b)], and the completion of reversal [Fig. 7(c)], is completed instantaneously. This process corresponds to the rapid jump in the hysteresis loop. While the reversal mechanisms for the polycrystalline and the epitaxial rings do

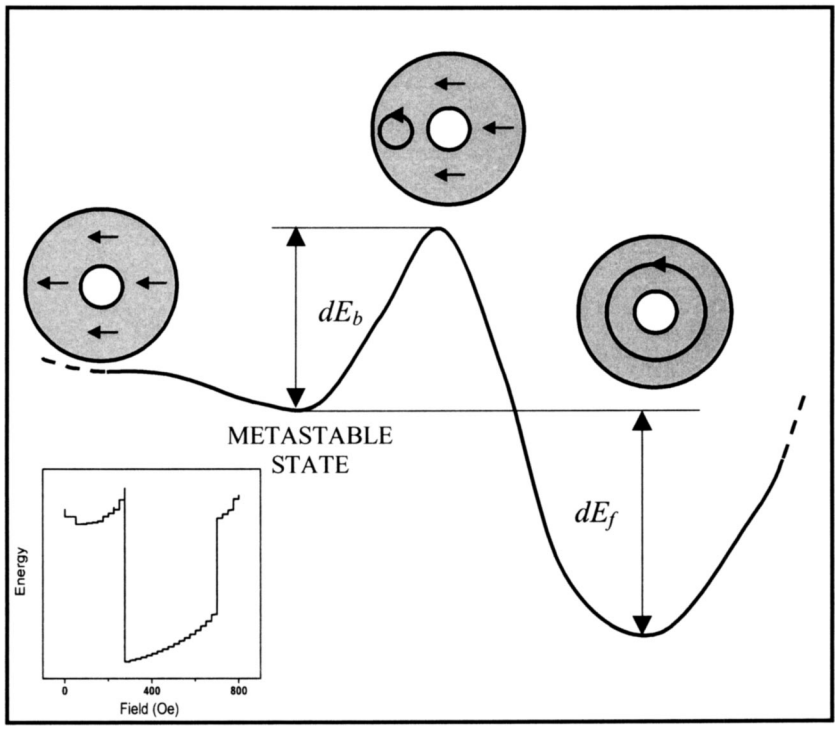

FIG. 6. Schematic illustration of energy distribution in different magnetic configurations of the ring. Inset is the total energy vs field plot obtained by simulation for a weak anisotropy ring. dE_b and dE_f are two definitions of energy barriers.

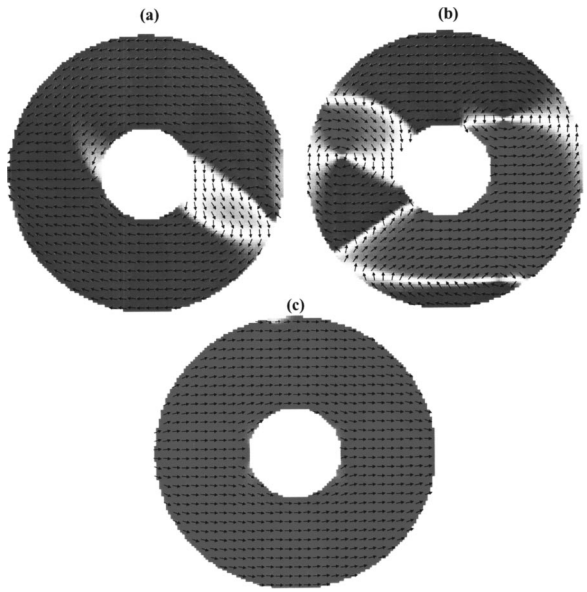

FIG. 7. Simulated magnetic configurations in the reversal process of an epitaxial ring. The processes are (a) buckling-like reversal, (b) local vortex nucleation, and (c) completion of reversal.

not vary significantly, they differ in the intermediate state. The most important feature is the absence of the intermediate stable vortex magnetic configuration from the reversal process of the epitaxial ring.

The question of whether the increase of magnetocrystalline anisotropy could render the vortex structure energetically unfavorable has also been examined by simulation. In the simulation, the magnetization of the epitaxial ring is forced into a vortex magnetic configuration and then saturated by an applied field. It has been found from an energy analysis that, although a large increase in anisotropy energy has been induced in the vortex state, it still cannot compensate the reduction of the demagnetizing energy caused by the transition from single domain to vortex state. Thus, the vortex magnetic configuration is still energetically stable in our epitaxial ring. However, such a stable state, which would result a jump in the hysteresis loop, has not been observed in the MOKE measurements. This can be understood as follows: the increase of the magnetocrystalline anisotropy has caused the change in total energy associated with the barrier dE_b (see Fig. 6), which has to be crossed for the transition from the metastable single domain to the vortex magnetic configuration, to become higher as a result of an anisotropy-induced barrier to local vortex formation. Magnetic moments in a material with strong magnetocrystalline anisotropy tend to align along the easy axis. Therefore, perturbations such as local vortex formation could increase the total energy. Furthermore, the magnetocrystalline anisotropy strongly increases the total energy of the vortex state in the nanomagnet. Consequently, the depth of the valley dE_f is reduced. When $dE_b > dE_f$, the vortex magnetic configuration can no longer appear in the reversal process. This is because the external field required to overcome the energy barrier is strong enough to force the magnetization directly from the metastable single-domain state into negative saturation, bypassing the vortex state.

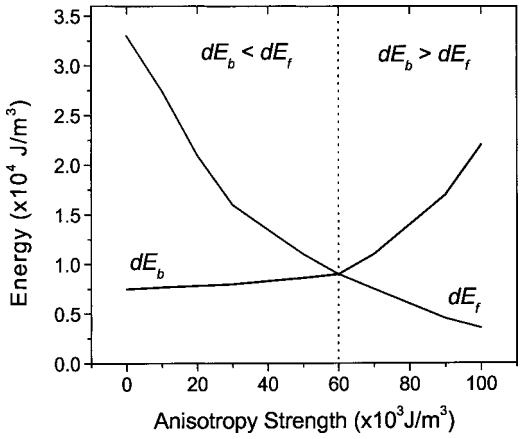

FIG. 8. Calculated evolution of dE_b and dE_f as functions of anisotropy strength, for 600 nm/200 nm outer/inner diameters, 20-nm-thick Co ring.

Figure 8 shows the calculated values of dE_b and dE_f as a function of anisotropy strength. When the anisotropy strength exceeds a critical value, the in-plane magnetization reversal does not have an intermediate vortex magnetic configuration. However, it is interesting to predict that if the dE_b value in our epitaxial sample can be decreased, it could be possible to have an intermediate vortex magnetic configuration in the reversal process. To test this prediction, hysteresis loop measurements were carried out along the directions away from the easy axis. Indeed, the appearance of the vortex magnetic configuration has been inferred from the measured MOKE hysteresis loop (see Fig. 9), which was measured with an applied field at an angle of ~70° with respect to the uniaxial easy axis. This result has also been confirmed in MFM imaging. After a demagnetizing treatment with a field perpendicular to the sample easy axis, a similar vortex MFM image has been observed [see Fig. 3(a)].

While numerical simulation can provide information about the evolution processes of the magnetization in ring nanomagnets, it is important to express the energies (anisot-

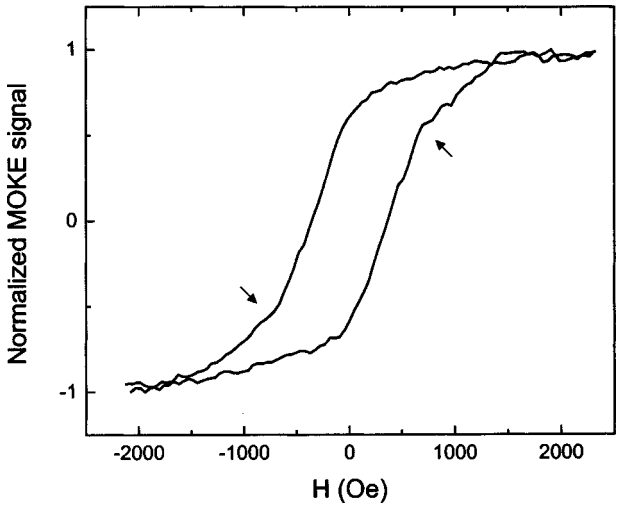

FIG. 9. MOKE loop measured from epitaxial ring nanomagnet with a field applied at an angle ~70° with respect to the easy axis. Arrows show switches in the loop, indicating the presence of vortex magnetic configuration.

ropy, exchange, and demagnetizing) analytically. For a single ring nanomagnet in the vortex magnetic configuration, the anisotropy energy density E_a can be derived as

$$E_a = \frac{2K_u}{\pi}\int_0^{(\pi/2)} \sin^2\theta d\theta = \frac{K_u}{2}, \tag{1}$$

where K_u is the uniaxial magnetic anisotropy constant and θ is the angle with respect to the uniaxial easy axis. From Eq. (1) one can obtain the same value of anisotropy energy as numerically calculated. One can see that the E_a value does not depend on the ring parameters. Therefore, the anisotropy energy could be important in certain circumstance, for instance, in a thinner ring, where it becomes a dominant term.

Although the exchange energy in a ring nanomagnet is not as strong as that in a disk-shaped nanomagnet, it can also be important in a thin and small ring. The exchange energy in a ring nanomagnet with a vortex magnetic configuration can be easily derived, unlike the complicated magnetization distribution in the vortex core[15] of a disk nanomagnet. When there is an angle φ between two spins S, the exchange energy is $-2AS^2\cos\varphi$. Consider a flux-closure spin circle with a radius r, and the distance between the two neighboring spins equal to the atomic distance of a material a_o. The total exchange energy in a single atomic ring is $AS^2 2\pi d/r$. After integrating over the whole ring structure, we obtain the energy density:

$$E_{\text{ex}} = \frac{nAS^2}{2a_o(R_o^2 - R_i^2)}\ln\frac{R_o}{R_i}, \tag{2}$$

where R_o and R_i are the external and inner diameters of the ring nanomagnet, respectively, and n is the number of the nearest neighbors of atoms in the material. The calculated exchange energy obtained from Eq. (2) agrees with the results of numerical simulations.

The most important energy that we need to derive is the demagnetizing energy. For the analysis of demagnetizing energy, a demagnetizing factor needs to be known. From a series of numerically simulated data,[23] we have extracted a relation between the demagnetizing factors of a ring (N_r) and a circular disk (N_d) as

$$\frac{N_r}{N_d} = \left(\frac{R_o}{R_o - R_i}\right)^{0.68}. \tag{3}$$

The values of the demagnetizing factors N_d for the disk with different ratios of height to diameter can be obtained from Ref. 24. We can then express the demagnetizing energy density as

$$E_d = \frac{1}{2}\mu_0\left(\frac{R_o}{R_o - R_i}\right)^{0.68} N_d M_s^2. \tag{4}$$

Although there is a singularity in Eq. (3) when $R_o \to R_i$, it gives a good approximation if the ring is not too narrow {for instance $[(R_o - R_i)/R_o > 0.1]$}. From Eq. (4), we can see that the magnetostatic energy closely depends on the inner diameter. For a narrow ring, after removing applied field, the magnetization is strongly constrained along the ring edge, and two head-to-head domains occur instead of two magnetic poles in a wide ring. Consequently, a wall propagation mechanism in the reversal process is expected.[8] By using the above equations, we have evaluated the energy in a 3-nm-thick Co ring with external and internal diameters of 150 nm and 50 nm, respectively. It was found that for the demagnetizing energy to compensate both the exchange and the anisotropy energy, the anisotropy strength K_u cannot be higher than 10^4 J/m^3: such a small anisotropy can be induced in a film by growing texture, stray field, etc. Otherwise, the vortex magnetic configuration would be energetically unstable in such a ring. Therefore, for sensor applications of ring magnets, the intrinsic anisotropy properties are very important; a strict control of material softness is likely to be a key issue.

IV. CONCLUSION

In summary, MOKE magnetometry and MFM imaging, combined with numerical micromagnetic simulations, have been used to study the influence of the magnetocrystalline anisotropy in the magnetization reversal of submicron Co rings. Under an in-plane applied field, the magnetization reversal of the ring nanomagnet starts from a buckling-like reverse domain nucleation, followed by local vortex formation, and an avalanche process of local vortex nucleation. For ring nanomagnets with a weak anisotropy, the complete magnetization reversal takes place via the transition from saturation at large negative fields, into a vortex magnetic configuration at small fields, and back into the reverse saturation state at large positive fields. By increasing the anisotropy strength above a critical value, the intermediate vortex magnetic configuration can be prevented from appearing; instead, the reversal occurs through a rapid jump. A strict control of material softness in submicron ring magnets is crucial, as a high magnetocrystalline anisotropy can lead to an unstable vortex magnetic structure.

ACKNOWLEDGMENTS

We thank T. Dimopoulos at the Institute de Physique et Chimie des Matériaux de Strasbourg for his technical assistance, and D. C. Hatton at the Cavendish Laboratory for useful discussions. One of the authors (W. S. L.) acknowledges the support of the Cambridge Commonwealth Trust.

[1] G. A. Prinz, Science **282**, 1660 (1998); C. A. Ross Annu. Rev. Mat. Res. **31**, 203 (2001); M. Johnson, IEEE Spectrum **37**, 33 (2000); S. P. Li, W. S. Lew, J. A. C. Bland, L. Lopez-Diaz, M. Natali, C. A. F. Vaz, and Y. Chen, Nature (London) **415**, 600 (2002).
[2] E. Gu, E. Ahmad, J. A. C. Bland, L. M. Brown, M. Rührig, A. J. McGibbon, and J. N. Chapman, Phys. Rev. B **57**, 7814 (1998).
[3] R. P. Cowburn, A. O. Adeyeye, and M. E. Welland, Phys. Rev. Lett. **81**, 5414 (1998).
[4] T. Shinjo, T. Okuno, R. Hassdorf, K. Shigeto, and T. Ono, Science **289**, 930 (2000).
[5] A. Fernandez and C. J. Cerjan, J. Appl. Phys. **87**, 1395 (2000).
[6] C. Mathieu, J. Jorzick, A. Frank, S. O. Demokritov, A. N. Slavin, and B. Hillebrands, Phys. Rev. Lett. **81**, 3968 (1998).
[7] C. Shearwood, S. J. Blundell, M. J. Baird, J. A. C. Bland, M. Gester, H. Ahmed, and P. H. Hughes, J. Appl. Phys. **75**, 5249 (1994).
[8] J. Rothman, M. Kläui, L. Lopez-Diaz, C. A. F. Vaz, A. Bleloch, J. A. C. Bland, Z. Cui, and R. Speaks, Phys. Rev. Lett. **86**, 1098 (2001).
[9] S. P. Li, D. Peyrade, M. Natali, A. Lebib, Y. Chen, U. Ebels, L. D. Buda, and K. Ounadjela, Phys. Rev. Lett. **86**, 1102 (2001).
[10] J. Zhu, Y. Zheng, and G. A. Prinz, J. Appl. Phys. **87**, 6668 (2000).

[11] G. A. Prinz, US Patent No. 54,774,824 (1995).
[12] L. Torres, E. Martinez, L. Lopez-Diaz, and J. Iñiguez, J. Appl. Phys. **89**, 7585 (2001).
[13] R. P. Cowburn and M. E. Welland, Appl. Phys. Lett. **72**, 2041 (1998); R. P. Cowburn and M. E. Welland, Phys. Rev. B **58**, 9217 (1998).
[14] R. P. Cowburn, D. K. Koltsov, A. O. Adeyeye, M. E. Welland, and D. M. Tricker, Phys. Rev. Lett. **81**, 5414 (1998).
[15] A. Hubert and R. Schäfer, *Magnetic Domains: The Analysis of Magnetic Microstructure* (Springer, Berlin, 1998).
[16] J. Raabe, R. Pulwey, R. Sattler, T. Schweinböck, J. Zweck, and D. Weiss, J. Appl. Phys. **88**, 4437 (2000).
[17] E. Gu, M. Gester, R. J. Hicken, C. Daboo, M. Tselepi, S. J. Gray, J. A. C. Bland, L. M. Brown, T. Thomson, and P. C. Riedi, Phys. Rev. B **52**, 14704 (1995).
[18] A. Lebib, M. Natali, S. Li, E. Cambril, L. Manin, Y. Chen, H. M. Janssen, and R. P. Sijbesma, Microelectron. Eng. **57–58**, 411 (2000).
[19] A 2D micromagnetic code developed by M. Donahue and D. Porter, NIST. Detail of the public domain program is available at http://math.nist.gov/oommf/
[20] A. Lebib, S. P. Li, M. Natali, and Y. Chen, J. Appl. Phys. **89**, 3892 (2001).
[21] J. F. Smyth, S. Schultz, D. R. Fredkin, D. P. Kern, S. A. Rishton, H. Schmid, M. Cali, and T. R. Koehler, J. Appl. Phys. **69**, 5262 (1991).
[22] R. Ferré, K. Ounadjela, J. M. George, L. Piraux, and S. Dubois, Phys. Rev. B **56**, 14066 (1997).
[23] W. S. Lew, S. P. Li, and J. A. C. Bland (unpublished).
[24] D. X. Chen, J. A. Brug, and R. B. Goldfarb, IEEE Trans. Magn. **27**, 3601 (1991).